Video Microscopy of Dynamically Aggregated Paramagnetic Particle Chains in an Applied Rotating Magnetic Field

Anil K. Vuppu,[†] Antonio A. Garcia,*[,†] and Mark A. Hayes[‡]

Department of Bioengineering, Arizona State University, Tempe, Arizona 85287, and Department of Chemistry and Biochemistry, and The Center for Solid State Electronics Research, Arizona State University, Tempe, Arizona 85287

Received February 4, 2003. In Final Form: August 4, 2003

A rotating unidirectional magnetic field generated by a motor-mounted permanent magnet was used to dynamically aggregate paramagnetic particles from suspension to form chains. Video microscopy and image processing were used to analyze the data. Good synchronicity was observed between the chains and the field up to 8 Hz frequency. Chain growth is facilitated at very low rotational frequencies initially after starting from static conditions, after which the mean chain length decreases in response to increasing viscous drag forces. As the frequency is increased from low values, the mean chain length decreases initially rapidly and later more slowly at higher frequencies, thus resulting in two regimes: the fast and the slow decrease regimes. Typical structures such as linear chains and S-shaped chains are observed as well as unusual U-shaped structures. The formation of dynamic S-shaped structures can be predicted based on the flexibility of the chains and the principle of conservation of angular momentum. Formation of single-chain aggregates is observed in microwells that are up to 50 μm wide, whereas in larger microwells multichain formation was noticed. The motor-mounted permanent magnet arrangement has applications in the development of portable microchip biosensors. The arrangement proved sufficient and reliable in forming chains, which display behavior similar to that observed under more elaborate and controlled conditions.

1. Introduction

A number of research studies[1] in recent years have focused on the creation of microelectromechanical (MEMS) devices. This is in line with the increased interest in miniature devices and their applications. A number of investigations are being conducted on the design of microfluidic devices, especially for biomedical and biochemical applications, such as the drug-delivery and lab-on-chip systems for point-of-care medical diagnostics.[1]

Earlier studies related to the work described here used semiconductor processing techniques[2] and electrodeposition techniques[3] to form solid microrotors that are capable of mixing small fluid volumes. Researchers have also started looking at particle aggregates for their suitability in micromixing as well as other microfluidic applications.[4] Recently, we have discovered a novel way of using paramagnetic particle aggregates for microfluidic biological and chemical detection applications,[5] wherein signals from the target molecules bound to the rotating chains are detected over the background noise. The use, in these detection devices, of particles that aggregate to form microrotors under an external magnetic field has several advantages such as dynamic assembly, dynamic variability in rotor length and speed, easy injection and extraction from the system, multiple use, and multitarget detection. In this paper, we report results from our studies on the formation and behavior of microrotors that dynamically aggregated from a colloidal suspension of paramagnetic particles upon the application of an external magnetic field using a rotating permanent magnet. This is a continuation of our investigations[4,5] into the patterning and applications of paramagnetic particles.

Colloidal suspensions of magnetically or electrically inducible microparticles are characterized as magnetorheological (MR) or electrorheological (ER) fluids, respectively.[6,7] Under an applied magnetic (or electric) field, these particles acquire an induced dipole moment causing them to aggregate and form supraparticle structures. Depending on the strength of the field and concentration of the particles, they aggregate in order to minimize the free energy of the system into one-, two-, or three-dimensional structures.[6−8] Under static conditions, the forces acting on the particles are the magnetic interaction force, excluded volume force, and thermal (i.e., Brownian) motion. The ratio of the magnetic interaction energy between particles to their thermal energy is given by the dimensionless term $\lambda = W_m/k_BT = \mu_0 m^2/(16\pi a^3 k_B T)$, where W_m is the magnetic interaction energy, μ_0 is the magnetic permeability in a vacuum, k_B is the Boltzmann constant, T is the temperature in Kelvin, a is the radius of the

* To whom correspondence should be addressed. E-mail: tony.garcia@asu.edu. Phone: (480) 965-8798. Fax: (480) 727-7624.
[†] Department of Bioengineering.
[‡] Department of Chemistry and Biochemistry, and The Center for Solid State Electronics Research.

(1) Hoch, H. C.; Jelinski, L. W.; Craighead, H. G. In *Nanofabrication and Biosystems*: *Integrating Materials Science, Engineering, and Biology*; Hoch, H. C., Jelinski, L. W., Craighead, H. G., Eds.; Cambridge University Press: Cambridge, 1996.
(2) Ahn, C. H.; Kim, Y. J.; Allen, M. G. *J. Microelectromech. Syst.* **1993**, *2* (4), 165.
(3) Barbic, M.; Mock, J. J.; Gray, A. P.; Schultz, S. *Appl. Phys. Lett.* **2001**, *79* (9), 1399−1401.
(4) Hayes, M. A.; Polson, N. A.; Garcia, A. A. *Langmuir* **2001**, *17* (9), 2866−2871.
(5) Vuppu, A.; Garcia, A.; Hayes, M.; Booksh, K.; Saha, S.; Phelan, P.; Calhoun, R. *J. Microelectromech. Syst.*, submitted.
(6) Halsey, T. C.; Martin, J. E.; Adolf, D. *Phys. Rev. Lett.* **1992**, *68* (10), 1519−1522.
(7) Melle, S.; Rubio, M. A.; Fuller, G. G. *Phys. Rev. Lett.* **2001**, *87* (11), 115501_115501−115501_115504.
(8) Martin, J. E.; Odinek, J.; Halsey, T. C. *Phys. Rev. Lett.* **1992**, *69* (10), 1524−1527.

10.1021/la034195a CCC: $25.00
Published on Web 08/30/2003

particle, and m is the induced magnetic moment.[9−12] The induced magnetic moment is given by the following equations: $m = (4/3)\pi a^3 \chi_{eff} \vec{H}$, $\chi_{eff} = 3(\mu_p - \mu_s)/(\mu_p + 2\mu_s)$, and $\mu_{p,s} = \mu_0(1 + \chi_{p,s})$ where μ_p and μ_s are the magnetic permeability of the particle and solvent and χ_p and χ_s are their respective magnetic susceptibilities. For our system, λ has been calculated to be in the range of 390−7500 (1−2 μm particle diameter, 45−70 G field), which implies that the magnetic interaction between particles dominates over thermal motion. In addition to static forces, the particles also experience hydrodynamic forces in a rotating field due to the rotational motion of the chains. The dynamic processes occurring in a rotating field have also been addressed for specific systems.[10,13,14]

Recently, Melle and colleagues[7,9,10,13] and Martin and colleagues[6,8,14−18] have conducted extensive theoretical and experimental studies to understand the behavior of MR and ER fluids under static and dynamic conditions.[6−17] Initial rheological studies and simulations were aimed at understanding the nature of the aggregation.[12,18−20] These experimental studies employed techniques such as optical scattering and dichroism to obtain a fundamental understanding of the order and kinetics of aggregation[7,8,10] and usually used very high particle volume fractions. During the past decade, researchers have begun to employ optical microscopy and lower particle concentrations to visualize the particle aggregates and verify their theoretical calculations.[9,11,21−25] Video microscopy not only helps in the verification of models but also enables the understanding of chain formation and growth processes, the dynamic behavior of chains, the statistical distribution of measured properties, and atypical structures that are not predicted in simulations since they are averaged out in statistical studies.

The previous experimental studies[9,10,13,20,26] make use of a set of Helmholtz coils, which are appropriately placed to generate a uniform rotating magnetic field at the center of the setup. However, this arrangement is not easily adaptable for portable microfluidic device applications that need a rotating field applied at the sample well. We have hence devised an alternative setup consisting of a neodymium−iron−boron rare-earth magnet mounted on a motor to provide the rotating magnetic field over the sample. This is a novel setup that has not been used before by others and carries advantages such as flexibility in placement over any area of the microchip, variation in field strength by controlling the magnet's distance from the sample, and the ability to tilt the rotational plane of the field. In this arrangement, it is expected that there will be some nonuniformity in the field in the x,y,z directions, and efforts are made to minimize its effect on chain behavior. Here we report results from our systematic research on the particle behavior in free drops using this alternate arrangement. A drop of paramagnetic particle suspension placed under an optical microscope is used as the magnetic fluid. The high-resolution video images captured with this rotating magnetic setup were used to analyze particle aggregation and to corroborate and quantify chain formation under these conditions. The results from both free-drop and microwell experiments indicate satisfactory particle aggregation and chain behavior. The predictable and verifiable results from this study are expected to help in the devising of accurate, sensitive, and portable particle-based microchip biosensors.

2. Experimental Section

2.1. Sample Preparation. Polystyrene paramagnetic microspheres with the following properties were used: 1−2 μm diameter, $\rho \approx 2 \times 10^3$ kg/m^3, ∼2.5 wt % concentration in water, amine functionalized on the surface, and containing greater than 20 wt % of iron oxide (Polysciences, Inc., Warrington, PA, catalog no. 18879). In the microspheres, the polystyrene surface matrix encapsulates the iron oxide crystallites (which are approximately 50 nm in size).

The particles are cleaned by first collecting them using a NdFeB magnet in a microcentrifuge vial. The supernatant liquid, containing the surfactant, is removed and replaced with an equal amount of deionized (DI) water, and the solution is vortexed for 10 min to resuspend the spheres. This procedure is repeated six times. The final three washings and resuspensions are carried out in 50% ethanol after which the spheres are resuspended in water to reconstitute the 2.5 wt % suspension.

Initial experiments at 2.5 wt % concentration resulted in large-scale aggregation of the microspheres toward the center of the particle suspension when placed under the magnet. After two successive dilutions, a concentration of 0.021 wt % was found to be satisfactory, and individual chains could be clearly seen. This concentration is equivalent to a volume fraction of $\phi = 1.05 \times 10^{-4}$ (assuming a density of 2×10^3 kg/m^3 for the paramagnetic microspheres), with a calculated particle concentration between 2×10^8 and 2.5×10^7 particles/mL for 1−2 μm microspheres, respectively. The suspension is shaken vigorously in a mixer−shaker before each sample is withdrawn. No settling of spheres was observed during the experimental runs as the duration of each run was only a few minutes and the magnetic field exerted an upward force during this time.

2.2. Experimental Setup and Procedure. A schematic of the experimental setup is shown in Figure 1. Experiments were carried out using an Olympus IX70 inverted research microscope (Tokyo, Japan) with a RS170 CCD camera (SCI Electronics, East Hartford, CT) connected to a Sony digital camcorder and a TV monitor. For fluorescence studies, a Leica DM IRB inverted microscope with an Optronics DEI-750D CE camera (CCD plus control unit) was connected to a JVC SR-VS20U video cassette recorder and TV monitor. All videos were captured at the standard video rate of 30 frames/s. A neodymium−iron−boron (NdFeB 27/30 mixed) rare-earth disk magnet (Edmund Scientific, NY, catalog no. CR30351-06), 1.9 cm in diameter, 0.5 cm thick, and rated at 11 lbs lift, was used to generate the external magnetic field. The magnet was mounted at the end of an approximately 7.6 cm long shaft connected to a small portable 24 V direct current (dc) gear case motor (Globe Industries Inc., Dayton, OH). The

(9) Melle, S.; Calderon, O. G.; Rubio, M. A.; Fuller, G. G. *J. Non-Newtonian Fluid Mech.* **2002**, *102* (2), 135−148.
(10) Melle, S.; Fuller, G. G.; Rubio, M. A. *Phys. Rev. E* **2000**, *61* (4), 4111−4117.
(11) Furst, E. M.; Suzuki, C.; Fermigier, M.; Gast, A. P. *Langmuir* **1998**, *14* (26), 7334−7336.
(12) Mohebi, M.; Jamasbi, N.; Liu, J. *Phys. Rev. E* **1996**, *54* (5), 5407−5413.
(13) Melle, S.; Rubio, M. A.; Fuller, G. G. *Int. J. Mod. Phys. B* **2001**, *15* (6−7), 758−766.
(14) Martin, J. E.; Anderson, R. A.; Tigges, C. P. *J. Chem. Phys.* **1998**, *108* (18), 7887−7900.
(15) Martin, J. E.; Odinek, J.; Halsey, T. C. *Phys. Rev. E* **1994**, *50* (4), 3263−3266.
(16) Martin, J. E.; Odinek, J. *Phys. Rev. Lett.* **1995**, *75* (15), 2827−2830.
(17) Martin, J. E.; Anderson, R. A. *J. Chem. Phys.* **1996**, *104* (12), 4814−4827.
(18) Martin, J. E.; Anderson, R. A.; Tigges, C. P. *J. Chem. Phys.* **1998**, *108* (9), 3765−3787.
(19) Halsey, T. C.; Toor, W. *Phys. Rev. Lett.* **1990**, *65* (22), 2820−2823.
(20) Melle, S.; Calderon, O. G.; Fuller, G. G.; Rubio, M. A. *J. Colloid Interface Sci.* **2002**, *247* (1), 200−209.
(21) Fraden, S.; Hurd, A.; Meyer, R. *Phys. Rev. Lett.* **1989**, *63* (21), 2373−2376.
(22) Fermigier, M.; Gast, A. *J. Colloid Interface Sci.* **1992**, *154* (2), 522−539.
(23) Wirtz, D.; Fermigier, M. *Phys. Rev. Lett.* **1994**, *72* (14), 2294−2297.
(24) Grasselli, Y.; Bossis, G.; Lemaire, E. *J. Phys. II* **1994**, *4* (2), 253−263.
(25) Promislow, J.; Gast, A.; Fermigier, M. *J. Chem. Phys.* **1995**, *102* (13), 5492−5498.
(26) Melle, S.; Calderon, O. G.; Rubio, M. A.; Fuller, G. G. *Int. J. Mod. Phys. B* **2002**, *16* (17), 2293−2299.

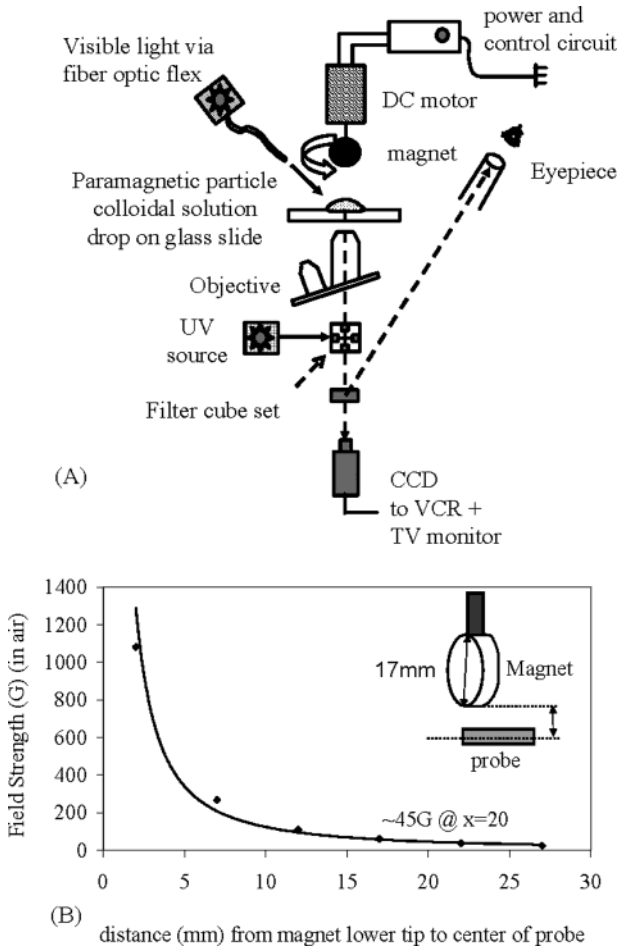

Figure 1. (A) Schematic of the experimental setup. (B) Variation of magnetic field strength with distance from the magnet. Experiments were conducted with a sample−magnet distance of 15−20 mm, which corresponds to a magnetic field strength of 45−70 G.

motor was controlled via a custom-designed circuit and ran on standard 120 V alternating current (ac) power. The motor can be operated at speeds varying from 5 to 460 rpm maximum. Specific rotational speeds were measured using a Monarch Pocket-Tach-plus tachometer (VWR International, CA, catalog no. 20904-107) with a range of 5−10000 rpm.

The experimental procedure consisted of placing an approximately 25 μL drop of the 0.021 wt % microsphere solution on a clean microscope glass slide that is mounted on the inverted microscope. The sample forms a hemispherical drop, about 7 mm in diameter, which is observed for the approximately 10 min duration of each experiment. For every new experimental measurement and motor setting, a fresh drop was placed in a different location on the glass slide, and care was taken to avoid measurements on almost dry drops that begin to show particle adhesion to the surface. The magnet/motor assembly is then brought into position so that the disk magnet is directly over the drop. In this setup, the magnet is rotating about an axis passing through its diameter, with the lower end of the magnet approximately 1.5−2 cm from the glass slide (Figure 1A). A plot of magnetic field strength versus distance from the tip of the magnet (Figure 1B) indicated that after an initial rapid decrease very close to the magnet's surface, the field changes slowly at moderate distances from the magnet. The field, as measured by a gauss meter, is estimated to be in the range of 45−70 G at distances of 1.5−2 cm directly below the magnet's surface. Further, at this vertical separation, the field strength at the edge of the sample drop (ca. radial distance of 5 mm in the *xy*-plane) is measured to be less by approximately 10 G as compared to that at the center. The extent of magnetization of the microspheres also varies due to the polydispersity in the microsphere size (1−2 μm) and with different magnetic particle content. Due to these reasons, it is possible that there is a nonuniformity in field and magnetization in the sample volume, and the above-mentioned range for field strength is expected to accommodate the nonuniformity in the system. Keeping the magnet in this range ensures that small discrepancies in positioning do not significantly affect the observed results. An external light source (an ordinary table lamp) was used to provide the necessary illumination for capturing the videos.

Since the NdFeB magnet mounted on the motor generates the rotating magnetic field, the motor speed consistency was verified by selecting nine different speeds. Five measurements were taken at each speed at 1 min intervals using the Pocket-Tach tachometer. Overall, the readings were consistent, with a maximum standard deviation of about 3 rpm observed at 200 rpm. The standard deviation did not exceed 2% of the rpm for the range of speeds studied, with most of them being normally less than 1%.

The videos captured were digitized using Adobe Premiere 6 (Adobe Systems Inc., CA) at 30 frames/s speed with sequential extraction of the individual frames. Subsequent measurements (such as angles, lengths, and position coordinates) were made using ImagePro Plus 4.5 (Media Cybernetics, MD) image analysis software. A brightness/contrast optimization routine in the software was used to enhance the images. An image of a 20 μm i.d. silica capillary captured on the inverted microscopes was used as the calibration scale for all measurements.

3. Results and Discussion

When the paramagnetic particle suspension is placed in an external magnetic field, the particles begin to aggregate. Figure 2A,C gives images from two different drops at the same particle concentration showing the particles form long chains along the magnetic flux lines. We observed that in a stationary nonrotational magnetic field, the chains move along the flux lines toward one another in a one-dimensional (1D) fashion, thus growing in length without any significant lateral motion. Melle et al.[7] commented that for low concentrations, the initial aggregation would be mainly diffusion limited and hence isotropic. However, at longer times (i.e., a few tens of seconds), the average length of the aggregates becomes larger than the distance between each other, and 1D behavior appears with the chains approaching each other head-to-head along the same line.[7] In Figure 2A,C, 1D behavior is suggested. Similar chain structures were observed in the other samples also prior to rotation.

When the magnetic field begins to rotate, the microsphere chains or microrotors also begin to rotate with the field in order to remain oriented in the direction of the field. In addition to the usual interparticle colloidal and magnetic forces acting between the particles in static fields, the rotational motion also introduces shear forces on the chains causing them to break up into smaller segments. In Figure 2B,D, chain breakage after some bending and contortion is evident. In this study, the segments formed at initial breakup do not correlate to static chain lengths and rotational speeds because the magnet motor is unsteady for the first few seconds after start-up. However, the motor attains a steady speed a few seconds after start-up and provides a stable rotating magnetic field.

Figure 3A−E is a sequence of images, 4/30 s apart in time, depicting the complete rotation of paramagnetic particle chains at a motor speed of 96 rpm. All the chains appear to be oriented in the general direction of the field, although with some variation in direction from chain to chain. Measurements were made on similar image sequences at different rotational speeds of the motor to determine the rotational frequency of the chains as well as their sizes. The frequency of the chains was determined by measuring the orientation angles of all the chains in

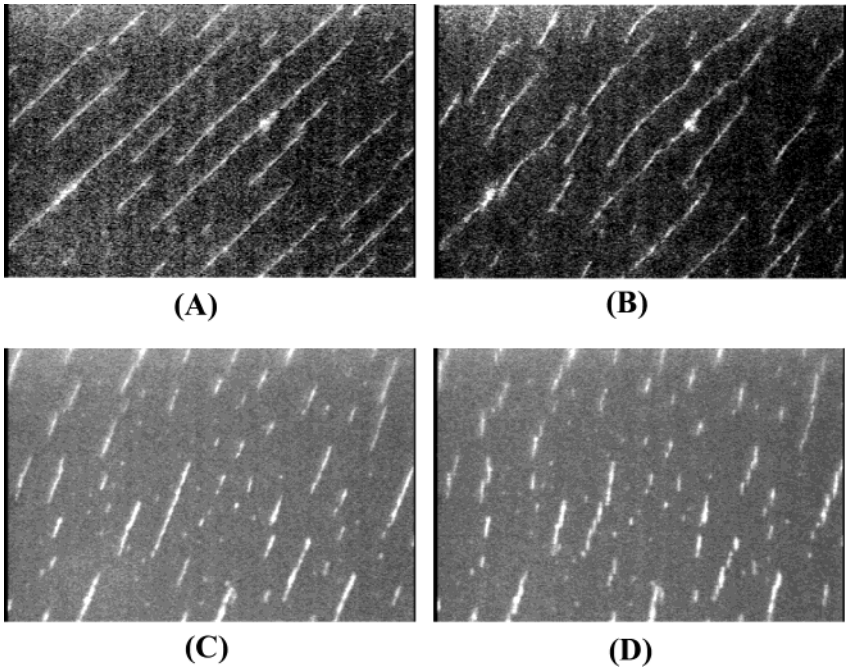

Figure 2. Images of paramagnetic microsphere chains in a magnetic field. (A,C) In a static field. (B,D) 1/30 s after the field starts rotating at 230 and 140 rpm, respectively.

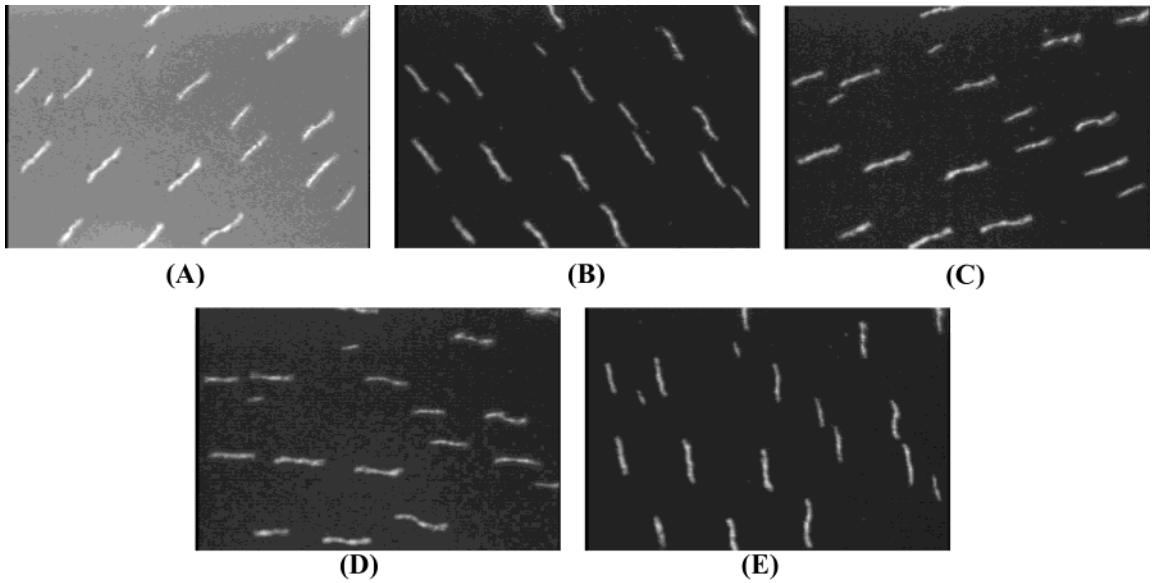

Figure 3. (A−E) Sequential images depicting chain rotation in anticlockwise sense at 96 rpm. The time difference between successive frames is 4/30 s.

each frame with respect to the vertical and plotting these mean orientation angles for sequential frames. Figure 4A is a typical graph of the mean orientation angles plotted for a series of sequential frames at a motor speed of 96 rpm. A linear fit to the data gives the slope to be 19.3° per frame, which equates to 96.5 rpm and is in good agreement with the frequency of the magnetic field expected by the magnet/motor assembly calibration using a strobe lamp. The linear fit with a regression coefficient of almost 1 observed in Figure 4A is also indicative of the steady rotation of the chains.

Mean orientation angle graphs, similar to Figure 4A, were made at different motor speeds, and the angular speeds of the chains were determined. These measurements, presented in Figure 4B, indicate good synchronization between the rotating magnetic field and the rotating chains or microrotors. Similar synchronization has been reported by other researchers[9] based on their video microscopy studies. From 345 to 460 rpm (which was the highest speed studied), the microrotor chains appear to lag by about 15 rpm as compared to the rotating magnetic field. However, this lag corresponds to approximately 3° and is well within experimental error. Synchronicity between the rotating magnetic field and the microrotors (Figure 4B) is expected even at high frequencies because, unlike a rigid body, particle chains are flexible and dynamic. They fragment into smaller segments in response to the increasing shear at higher speeds, while continuing to stay in-step with the magnetic field.[10]

Analysis of the orientation angles of all the chains in a frame indicates that the standard deviation is of the range of 2−10° within each frame, with larger deviations observed at higher rotational frequencies (Figure 4B). Uncertainty is introduced due to the error in determining

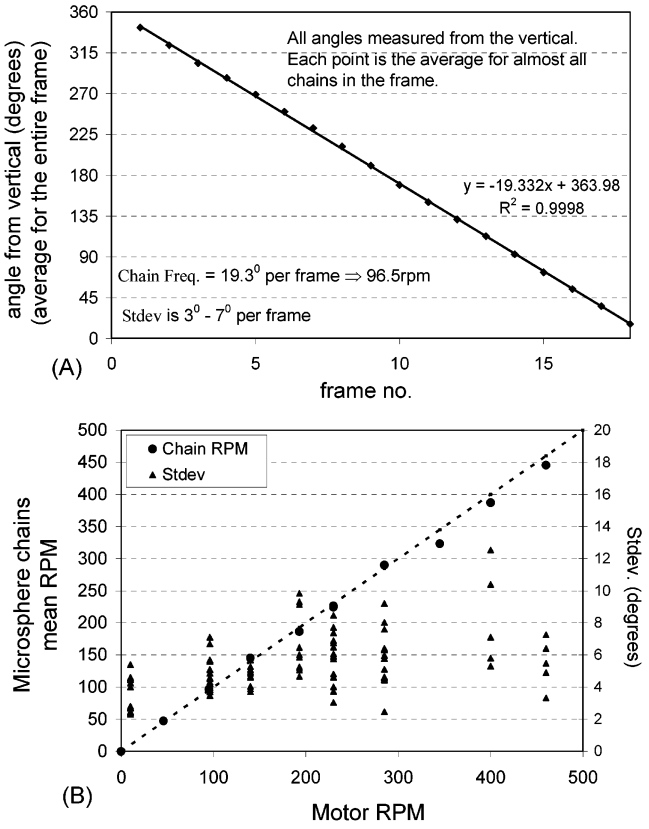

Figure 4. (A) Determination of the chain rotational frequencies by plotting the mean orientation angles of the chains for a sequence of images at 96 rpm. (B) Frequency comparison of the rotating magnetic field vs the measured rotational speed of the microsphere chains, which indicates good synchronization. The standard deviations, calculated over all chains within each frame, are in the range of 2−10°.

the orientation angles of chains with finite width, especially those that are S-shaped and nonlinear. This is especially true at higher rotational speeds when the fast-moving chains become comparatively shorter in length and appear blurred in the still frames, introducing slightly larger errors in angle measurements.

The rotating chains are observed to undergo a process of dynamic chain growth and fragmentation that is dependent on the frequency of the field. Chain growth was observed due to the overlapping of the chains as they rotate and by the 1D growth process that occurs when two neighboring chains align lengthwise head-to-head with each other. This process is depicted in a sequence of images in Figure 5 that were captured at the low frequency of 5 rpm. As the chains align lengthwise during rotation, they also move toward each other due to the attractive magnetic forces among the chains. As observed in Figure 5A−D, the final length in this case is the sum of the lengths of the approaching fragments. The viscous forces at these speeds are low enough to avoid chain fragmentation, and aggregates such as those in Figure 5D are stable until fragmentation due to either interaction with other chains or increased rotational frequency.

On the other hand, at very high rotational speeds the neighboring chains approach each other and separate quickly. The magnetic attractive forces at the ends of the chains appear to be insufficient to hold them together against the disruptive viscous forces. For a short time, the chains are attached end-to-end and act as one. This phenomenon can be observed in the sequence of images in Figure 6. The blur in these images, as mentioned earlier, is an optical effect due to the high tangential velocities at the ends of the chains. Since the chains can align head-to-head twice for each complete rotation of the field, the dynamic growth and fragmentation process has a frequency twice that of the field frequency. Melle et al.,[9] on the basis of the power-spectral analysis from their simulation studies, have also reported the oscillation in chain length to be twice the rotating field frequency.

Two interesting observations can be made by following the orientation and shapes of the dynamic structures in Figure 6A−D. The adjacent chains that merge momentarily to form a longer structure are out of phase, that is, aligned in a different direction, when compared to the other individual chains in the frame but attain the same orientation as the rest of the chains after fragmentation. In addition, the paramagnetic chains form S-shaped structures during the dynamic growth−fragmentation process, as noted by some other researchers also.[26,27] Our hypothesis on why these phenomena occur is based on consideration of the interplay between angular momentum conservation and the rotating magnetic field. The angular momentum (L) of a thin rodlike structure is equal to $I\omega$, where I is the moment of inertia of the rod given by the formula $I = kl^3/12$, where k is the linear density of the rod, l is the length of the rod, and ω is the angular velocity of rotation about a diametrical axis at the center of the rod. According to angular momentum conservation principles, the sum of the angular momentums of the two chain fragments should equal the angular momentum of the final enjoined chain,

$$L_i = L_f$$

$$L_1 + L_2 = L_f$$

$$I_1\omega_i + I_2\omega_i = I_f\omega_f$$

$$k{l_1}^3\omega_i + k{l_2}^3\omega_i = k{l_f}^3\omega_f$$

$$\omega_f = \frac{{l_1}^3 + {l_2}^3}{({l_f})^3}\omega_i = \frac{{l_1}^3 + {l_2}^3}{(l_1 + l_2)^3}\omega_i$$

In the above equations, the subscripts 1, 2, i, and f represent the chain fragments 1 and 2, before (initial) and after (final) the joining process, respectively. Thus when two rodlike structures rotating about their centers with similar angular velocities are joined, the angular velocity of the total structure reduces in order to conserve angular momentum. This slowing down is the reason that the final enjoined structure is out of phase relative to the other chains in the captured frame.

Melle et al.[10,13] have reported a frequency-dependent phase lag between the long axis of the chains and the magnetic field direction. This lag arises due to the balance between the driving magnetic torque and the resisting hydrodynamic torque on the chains. However, the additional lag induced by the slowing of the chain mentioned above would increase the magnetic torque on the chain and also the stress in the chain. Since the ends of the chain are hinged at only one end and have some flexibility, they can be expected to align with the field relatively quicker than the rest of the chain body, thus resulting in the S-shapes. However, the additional stress due to the increased phase lag would cause the chain to fragment after a certain critical point is reached during the course

(27) Melle, S.; Martin, J. E. *J. Chem. Phys.* **2003**, *118* (21), 9875−9881.

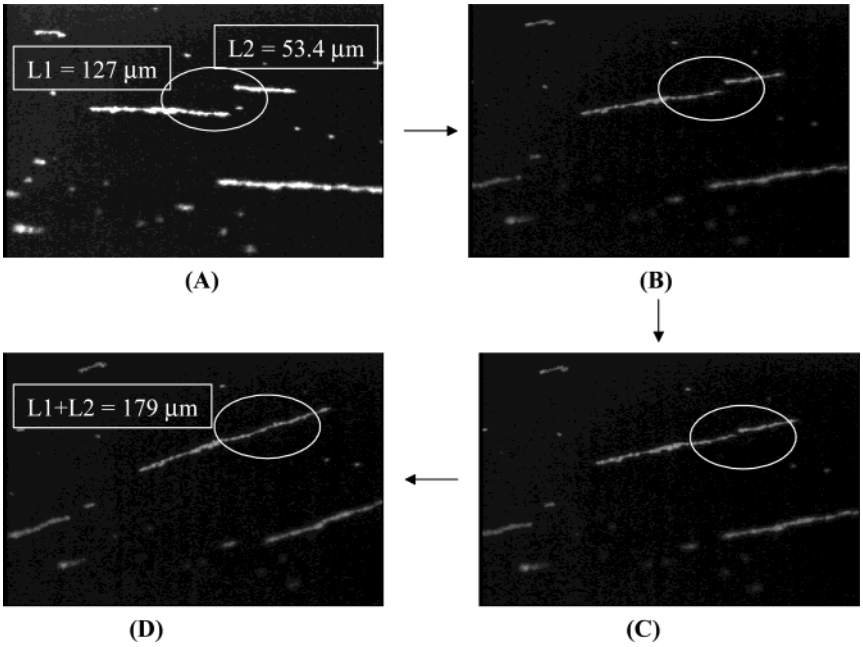

Figure 5. Sequential images depicting chain growth at a very low field frequency of 5 rpm. The slow rotation promotes 1D chain growth by aligning distant chains head-to-head lengthwise, helping aggregation. (A−D) The time differences between successive images are 25/30, 5/30, and 20/30 s.

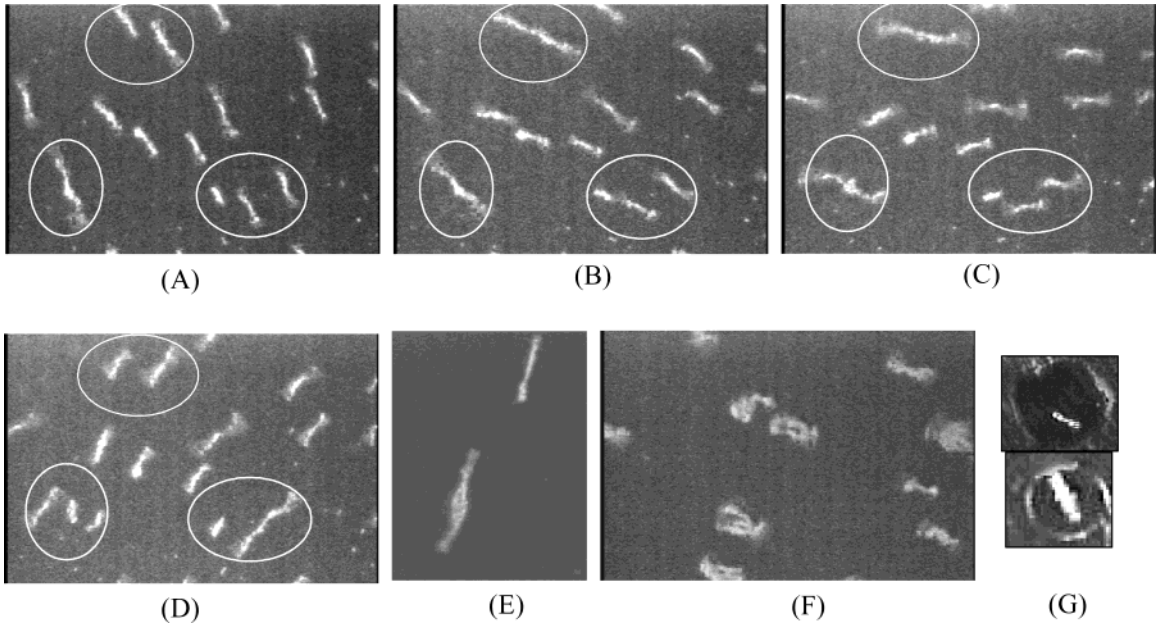

Figure 6. (A−D) Dynamic growth and fragmentation of chains at a high rotational frequency of 193 rpm. Neighboring chains momentarily attract when they line up head-to-head before they fragment again. This process repeats itself with regularity, at a frequency twice that of the rotating field. (E) A stable S-shape formed from overlapping chains at 95 rpm. (F) Stable U-shaped structures at 286 rpm. (G) A single chain formed in ~10 μm wide circular and square microwells observed at different magnifications. The wells are 12 μm deep.

of rotation. Melle et al.[10] give a critical angle for chain fragmentation to be 54.7°.

The lengths of a number of microsphere chains measured at different rotational speeds are graphed in Figure 7 and compared with data obtained from the study of Melle et al.[9] At lower rpm's ($\lesssim$70), some of the chains are longer than the capture window and the mean chain lengths at lower frequencies are skewed toward the lower values. Further, it can also be observed in Figure 7 that the decrease in chain length at increasing rotational speeds falls in two regimes. In the first regime observed at low rotational speeds of up to approximately 70 rpm, the mean chain length decreases rapidly from ~140 μm (at 5 rpm) to ~80 μm (at 70 rpm), after which the length decreases slowly, in absolute value terms, at the higher rotational frequencies comprising the second regime. The chain length at higher frequencies (~300−460 rpm) in this study is in the range of 35−55 μm. The power-law trend observed in this study is similar to those noted by Melle et al.[9] in their experimental and simulation studies. It can be observed that the mean chain lengths measured in this study are larger than those from their experiments. This difference is probably due to the difference in the experimental conditions used, such as the magnetic field strength and uniformity, the fluid cell dimensions, the solvent medium used, and the microsphere size. These

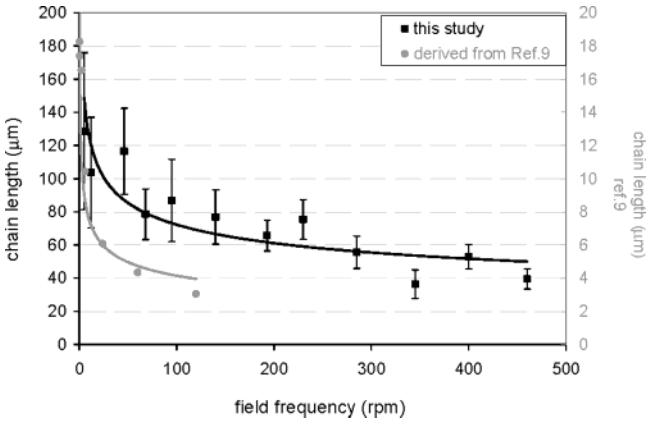

Figure 7. Plot of chain length variation with magnetic field rotational frequency: (■) data from this study; (●) data from ref 9. The solid curves represent best fit lines.

variables determine the interparticle attraction and the fluid drag forces on the chains, thus affecting the chain length. Our experimental measurements for chain lengths also closely match the results from our three-dimensional simulation studies[28] for a rotating planar magnetic field. This indicates that the effect of the nonuniformity of the magnetic field in our experiments appears not to affect chain length and its growth/fragmentation process significantly. The slow change of chain length at higher rpm's (>200 rpm) and the small variation at any particular rpm provide an ideal range of operation for consistent and reliable chain formation that is needed for our rotating magnetic chain biosensors.[5]

Microscopy studies also reveal some unusual structures that reflect the strength of the interparticle magnetic forces and the flexibility of the chains. The ability of particle aggregates in a rotating magnetic field to take other shapes is evident in Figure 6E,F. The left image shows a stable S-shape, which appears to have been formed by the joining of two overlapping chains that likely overlapped each other during rotation. Unlike the S-structures that dynamically form and fragment, this structure is stable, probably due to the overlap in the middle region, which would increase the interparticle magnetic forces thus preventing fragmentation. We have also observed some U-shaped structures, shown in Figure 6F, that appear to rotate about their center of mass visually creating a pinwheel-like effect. It is not clear what process could lead to the chain folding over itself to form the U-structures in a rotating magnetic field. Another process that was observed due to the interaction of the induced magnetism of the chains is the satellite-like behavior between two chain structures. In this case, a smaller structure orbits the larger one, even as both continue to rotate about their individual axes until they eventually form a larger aggregate. Such orbiting would involve translatory motion of the chain, which is observed in some other chains as well. This is probably due to a combination of the local variation in field and second-order effects due to neighboring chains. The effective functioning of the particle-based biosensors demands the understanding and minimization of such unusual structures, since such unusual chain behavior contributes to signal distortion. Apart from the free drop experiments, we have also been working with achieving controlled chain formation behavior in individual microwells. Figure 6G shows two single chains formed in circular as well as square wells that are approximately 10 μm wide and 12 μm deep. Similar single chains were observed for well widths of up to 50 μm, whereas for larger microwells multichain formation was noticed. An advantage of using the experimental setup mentioned in this study, of a motor-mounted permanent magnet, has been that the plane of rotation of the chains could be altered from horizontal (*xy*) to vertical (*xz* or *yz*) by simple tilting of the motor plus magnet assembly. This has provided us with two different approaches to signal derivation and analysis in our particle biosensor design.[5] Further research is ongoing with this experimental setup for attaining automated lock onto the rotating chains and signal analysis.

(28) Saha, S.; Vuppu, A.; Phelan, P.; Calhoun, R.; Garcia, A.; Hayes, M. *Sens. Actuators, B*, submitted.

4. Conclusions

A simple mechanical setup using a rare-earth magnet mounted on a gear case motor, for providing the external rotating magnetic field, was used to aggregate and orient paramagnetic polystyrene microspheres in suspension. While the applied field is slightly nonuniform, this arrangement however allows the flexibility needed for use in portable microchip biosensor applications. The video microscopy images captured were digitized, and measurements were made to observe and analyze the particle aggregates' behavior. Chain formation, growth and fragmentation, and the shapes and sizes of the chains were studied in free drops, and single-chain formation was studied in microwells. Results were compared with those from other studies that used more controlled conditions for chain formation.

In a unidirectional static magnetic field, the particles aggregate to form long one-dimensional chains from a dilute suspension of the microspheres. When the field is rotated, the chains fragment due to the shear forces acting on them, to attain an equilibrium distribution of chain lengths. At very low rotational frequencies, chain growth occurs due to the rotation, which provides an opportunity for distant chains to approach each other. At slightly higher and at intermediate frequencies, the chain lengths decrease rapidly due to the increasing viscous forces, whereas the chain lengths decrease slowly at higher frequencies, following a power-law behavior. The chains are synchronous with the changing field direction for the frequencies studied and adjust their size dynamically to balance the viscous forces. The small change in chain length with frequency at higher frequencies and the smaller variation provide a region of operation with consistent and reliable chain behavior that has biosensor and micromixing applications.

The flexibility of the chains in responding to the magnetic and drag forces acting on them results in some interesting structures such as S- and U-shapes. Dynamic S-shapes are observed at moderately high field frequencies when two rotating chains approach each other close enough for them to be momentarily attracted before they separate again. These shapes are a result of the reduced rotation of the enjoined structure due to conservation of momentum and due to the flexibility of the chain ends. Some stable S-shapes are observed to contain overlapping chains. In microwell studies, single-chain formation was observed in smaller microwells up to 50 μm width, whereas multiple chains were observed in larger wells. The lengths of the single chains in our experiments were smaller than the well width.

Our results compare well with those of previous electromagnet studies and show that permanent magnets mounted on a motor can form particle chains with similar behavior. Externally mounted rotating magnets have other advantages such as flexibility of the rotating field axes by

simply tilting the motor shaft, variability in field strength by changing the distance to the sample, and generation of a field at different locations on a microfluidic chip. This flexibility is of use in microfluidic applications and would reduce the complexity in the design and manufacture of on-chip magnetic fields.

Acknowledgment. The authors acknowledge the help of Evert Fruitman, of the Electrical Shop in the Department of Chemistry, in building the circuit and components of the gear case motor's controller box.

LA034195A